# EXPERIMENTAL ANALYSIS OF THE AERODYNAMICS OF POROUS FLAP SIDE-EDGE

F. P. Moraleda \*, F. M. Catalano\*\*
\*UPM –Madrid-Spain, \*\*Aeronautical Engineering Depto EESC-USP Brazil

**Keywords**: flap side-edge vortex, porous wing tip, experimental aerodynamics

#### **Abstract**

Experimental tests were performed to investigate the flow near a flap side-edge with attached porous plate as a potential noise reduction device. The experiments performed using only a wing to simplify the installation. The objective was to perform a first approximation to the flow field produced by the addition of porosity of different sizes. Baseline conditions and plates of 10mm, 20mm, 30mm, 50mm and 70mm placed in the bottom side of the wing tip were tested. Also, another configuration was tested, with a plate of 25mm roughly placed in the attachment line of the Aerodvnamic experiments vortex. performed to evaluate the changes in the lift, drag and pitching moment coefficients. Hot wire anemometry measurements were performed in perpendicular planes to the direction of the undisturbed flow. The porous plate transforms the structure of the vortex by dramatically decreasing the axial velocity in the core center transforming the tip vortex from a jet vortex to a wake vortex. Vorticity was also changed with a noticeable decrease. From 30mm porous strip, this decrease becomes asymptotic. The 50mm and 70mm plates show a merging between the wake and the vortex. The addition of the porous plate weakens the mechanisms of noise production as it reduces vorticity, core flow velocity and displaces it away to the wing tip.

#### 1 Introduction

The noise produced for the aircrafts become a more significant constraint in the design in the last years, due to the new normative and the high rate of growing of the civil aviation. The advances in engine technology achieved a significant reduction in engine noise that put the airframe noise in the spotlight. The noise produced by the aircrafts becomes a more and more serious problem with the increase of the civil aviation. For many years, the critical source of noise was the aircraft engine. Around 1970, the introduction of high-bypass engine ratio for fuel saving becomes in an important reduction of the noise. The aircraft noise became the bottleneck for noise reduction and was put into the spotlight [6]. Studies about the aircraft noise began, whether developing empirical models, either searching methods to reduce it. However, it was in the last years that the main actors put in the noise reduction. attention the NASA's Advanced Subsonic Technology (AST) program starts in 1995 and supposed a considerable effort to reduce noise [11]. The aim is to reduce noise one half respects to 1997 technology within 10 years and three quarters (20 dB) within 25 years [7]. Whereas, the European Comunity proposed reductions in the noise to one half in respect to 2000 technology which as included in the objectives of the "Vision for 2020". The Projeto Aeronave Silenciosa (Silent Aircraft Project) [12] is another example of the effort that is being done in this direction. The present work is included in the framework of the investigations of this project. The airframe noise is especially significant during the approach, when the engines are throttled down, and the high-lift devices are deployed. The major sources of noise are the landing gear, the spoilers and the high-light devices situated both in the leading and the trailing edge, like slats and flaps [11]. A number of projects to reduce this type of noise were developed for the major

actors in aeronautics. One of the most promising methods developed in the project Aeronave Silenciosa is the use of a porous plate to lessen the noise produced for the flap side-edge. A three element high lift wing with different sizes of porous plate attached to the flap side-edge was tested and an appreciable diminution in noise was achieved [5]. Nevertheless, the mechanism of noise reduction was not fully understood. In the present work a simple wing with various sizes of porous plate attached to its tip was tested to improve the knowledge about the physical process. Aerodynamic forces were also measured, as well as the flow field in a plane perpendicular to free stream velocity, using 3D hot-wire probe. The aim is to have a first understanding of the porous plate effect in a tip vortex, although the physical process is not exactly the same in a wing that in a flap. The field of study is quite large, and this work should be extended with more testing. The main source of noise in the flap is the side-edge, where a strong vortex is produced due to the difference in lift between flapped and unflapped sections (Fig. 1). This vortex is feeding with vorticity from the cylindrical shear layer. Both experimental and computational studies confirm this fact [2, 5, 3, 13]. Consequently, all of the literature about flap noise is about flap sideedge noise. The noise produced is present in a large range of frequencies that makes more difficult the study especially with computational methods [11]. All of the works agree with the idea [5]: there is a 2-vortex system, one smaller located at the top surface and one stronger at the bottom one, attached to the side-edge. The structure of the vortices can be seen at Fig. 1. The vortex resulting of the merger of these two is one of the fundamental sources of noise. This merging happens around at the mid-chord. The computational analysis of [6] mentions four sources of noise: free shear layers and their rollup, formation of multiple vortices, vortex merging and vortex bursting. The previous mechanism is only produced when the flap deflection reaches a critical value.

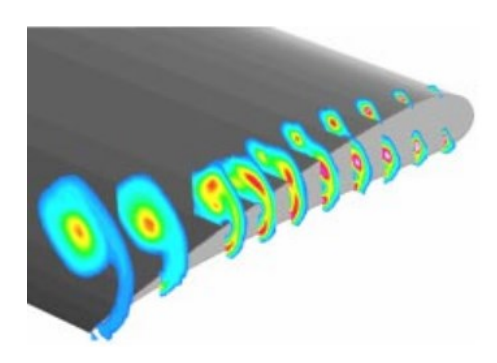


Fig. 1 Contours of streamwise vorticity. [11].

article mentioned particularly relevant for this work, because it analyzes how the flow field is changed with the introducing of a porous plate. The article of [11] focused in the mechanisms of noise generation in the wing flaps. Analyzing the potential instabilities of the flow, it proposes five sources of noise: 1) large-scale flow fluctuations due to the free-shear layer, 2) large scale flow fluctuations due to the post-merged vortex downstream, 3) convection of the turbulent boundary layer, 4) vortex merging and 5) vortex bursting. Only two of these mechanisms are studied, considered as the most potentially unstable, 1) and 2). The first refers to the shear layer that emanates from the flap bottom edge and spans the entire flap chord. The second one refers to the vortex produced by the merge of the two initial vortices, roughly in the midchord region. The fifth mechanism, the vortex breakdown, only appears when there is a significant adverse pressure gradient, that is, when the angle of attack is high enough. In this case, it can be dominant. The ultimate goal of this work is the study of the noise produced by the flap side-edge. Nevertheless, the research was focused in the alterations of the tip vortex with the addition of a porous plate. The aim is translating this knowledge to the real case of a complete wing with a high-lift system. This fact led to examine some of the literature related with the vortex, even though it is not related with noise. A short review of these references is done in this section. References about vortex measurements with a porous plate in the wingtip were not found. The paper of [8] presents a review of the investigations in Europe about commercial aircraft wake vortices. This study is far from the subject of work, but the article

presents some interesting recommendations about how to study the vortex. It recommends some formulas about the calculation of the center of the vortex, the circulation and other parameters that describe the structure of the vortex. Also, it presents some advices about how to define non-dimensional time and distance from the evolution of the vortex. The master thesis of [9] measures the vortex produced in the wing of a Micro-Air Vehicle (MAV). The same three-sensor anemometer was used to perform the measurements that support the primary interesting of this work. It can proportionate a reference to compare the results of the baseline conditions and also about the methods to perform the calibration. The research of [1] shows some interesting results that can be useful for the analyzing of the results of this work. It confirms the existence of various vortices produced in the end of the flat end-cap. These vortices move downstream around a common center until they merge to form a single vortex. Another attractive idea is the suggestion of two types of vortex: "jet-like" vortex or "wake like", depending on the axial velocity in the center is bigger or smaller than the free-stream velocity U∞. This differentiation is governed by the loading parameter,  $\Gamma/U\infty c$ , where  $\Gamma$  is the circulation and c the airfoil chord. In this work, the wing without porous plate produces a "jet-like" vortex, but the addition of it transforms the vortex into a "wake-like"

### 2 Experimental Set-up.

Wind tunnel LAE-1 of the The Aerodynamics Laboratory of the Aeronautical Engineering Department of University of São Paulo, was used for the tests. All of the information present in this section can be found in [4]. The working section of the tunnel is 1:30m high and 1:70m wide, with a usable length of 3m. This working section is involved by a room or plenum chamber made of concrete, in order to ensure that the static pressure of the chamber is equal to the atmospheric pressure. The flow is driven though an electric motor of 110HP with 8 blades and 7 straighteners. The blades of the motor are carefully designed to

obtain a high aerodynamic efficiency with low noise. The velocity is in the range of 10m/s to 55m/s, with a turbulence level of 0.21%. The turbulence of the tunnel, when it was constructed, was 0.25%. The reduction to 0.21% was achieved after the aeroacoustic update. The contraction ratio of the tunnel is 1:8. There are two 54% porosity nylon screens to reduce turbulence. The main instrumentation composed of a six component sting balance. three components underneath balance, digital pressure scanivalves and a three-channel hot wire anemometer. This anemometer includes a 3D transverse gear, and it was used extensively during this experiments.

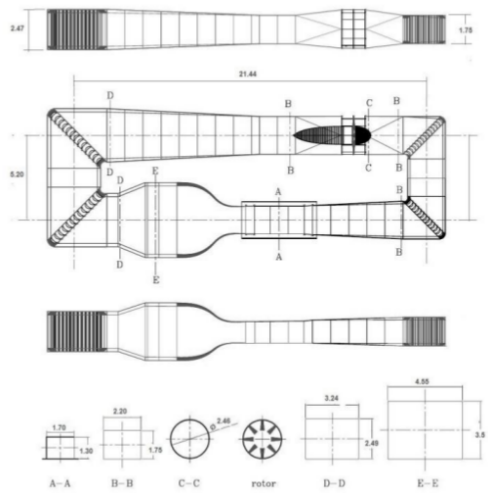


Fig. 2 Wind Tunnel layout.

The wing employed in the experiments has a chord c of 0:3m and a wingspan b of 0:45m. The airfoil of the wing is not a standard profile. It was generated in the framework of an investigation of a wind generator. The profiles of the root and tip were optimized with a genetic algorithm following a series of criteria. The airfoil employed corresponds to the intermediate profile between the root and the tip. It was chosen due to its availability at the laboratory and its shape that is relatively similar to a flap. The maximum thickness is 10% of the chord, that is, 30mm. The wing has a trip-strip in the leading-edge, in order to advance the turbulent transition and avoid complex flows with reattachment zones. The trip-strip is placed at 7% of the chord and has a width of 10mm. The porous plate is the same used for the last tests [5]. The plate has a 33% of porosity, with holes of 0:75mm of diameter and 1mm of thickness.

Two possible positions of the porous plate were examined. The first one corresponds to the best result obtained in the past experiments, with the plate in the pressure side. This configuration showed the best decreasing in noise and also is compatible with the existing flap configurations. The other configuration that was studied is the attach case, in which the porous plate is roughly in the attachment line of the bottom vortex. Photography of each placement of the plate can be seen in Fig. 3. Several widths (d) of the plate were examined. For the standard case, six different widths were studied: baseline, 10mm, 20mm, 30mm, 50mm and 70mm. For the attach case, only one width of 25mm was studied. In the precedent work [5] the maximum width examined was 15mm, with a chord c of 0.5m. This implies a non-dimensional width of d/c =0.03, while in this work it was reached a maximum of d/c = 0.23. The purpose is to study a wide range of sizes, to understand the entire physical process.

#### 2.1 Hot-wire Implementation.

The correct employ and calibration of the 3D hot-wire probe was the most important problem during the development of the present work. It was used the software included with the hotwire system, the Streamware v5.0. Apart from other functionalities, this software converts the voltages of each wire, the raw data, to 3D velocity data available for the user. However, problems related with this post-processing were founded along the testes. The experimental installation is formed for a triple-sensor probe with a traverse gear that allows 3D movement. Also a single-sensor probe was used in some tests. All of the instruments were supplied by DANTEC Dynamics. The most relevant devices are: Triple-sensor probe 55P91, the general aspect of the probe can be seen in Fig. 4, with also an explanation of the relative position of the axes; single-sensor probe 55P01; NI DAQCard-6036E; Streamline 90N10 frame with three CTA Modules 90C10 and the traverse gear.

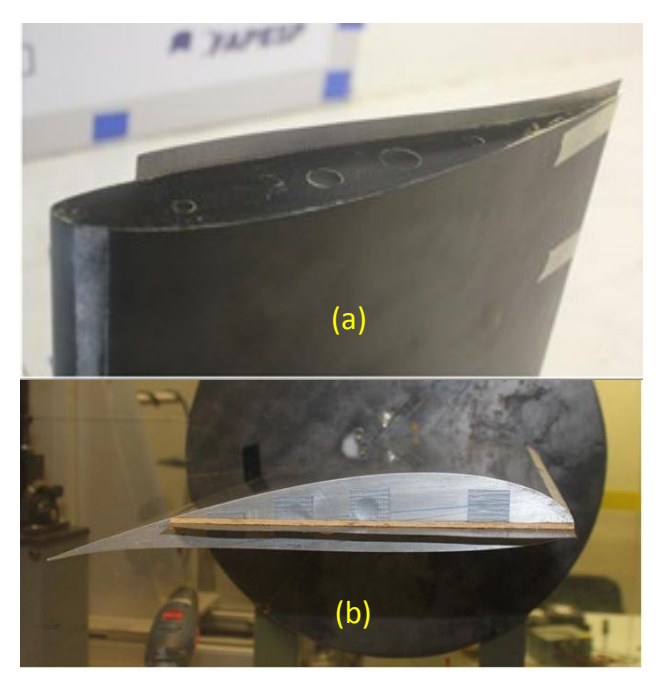


Fig. 3 Standard configuration (a) Position of the plate for the attach configuration (b).

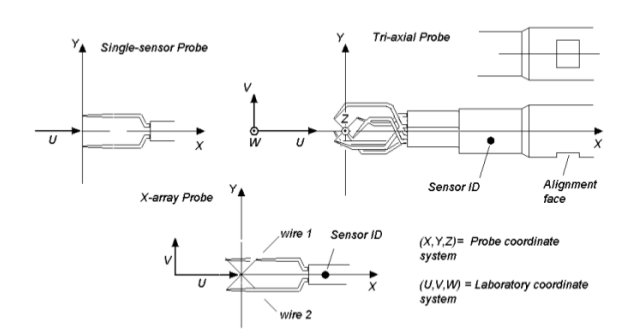


Fig. 4 Hot wire probe coordinates.

It was checked that this configuration is sufficient to capture the mean values of the flow field. The raw data have to be transformed in velocity expressed in laboratory coordinates. The tool to do this in Streamware is called Data Conversion. The other important transformation is the Data Reduction. It consists in convert the multiple data for each position in statistical values. It can be done before or after the Data Conversion. The most relevant statistical values provided to the program are the mean value Xmean and the standard deviation Xrms:

$$X_{mean} = \frac{1}{N} \sum_{i=1}^{N} X_{i}; \qquad X_{rms} = \left(\frac{1}{N-1} \sum_{i=1}^{N} (X_{i} - X_{mean})^{2}\right)^{0.5}$$
 (1)

Where N is the number of samples (1024, in this case) and Xi are the different measures. X can be anyone of the data

mentioned before, as voltage, velocity in wire coordinates or velocity in laboratory coordinates. The standard deviation is used to evaluate the turbulence in each point. It is necessary be careful with the next fact: the statistical result of a transformed value is not the same that the transformed of the statistical result. That is, to calculate the mean of the laboratory coordinates, it is necessary to execute the transformation over all of the samples and then calculate the mean value. During the experiments, problems were observed with the Data Reduction and Conversion done by the program. Different results were obtained for the same set up and also non-sense results were obtained. It was not clear if this was due to an incorrect use of the software, errors present in the program or a combination of both. In any case, it was developed an own algorithm to post-process the data, based in the formulas presented in the manual. The principal advantage of the algorithm developed is its transparency. While the problems with the DANTEC software still not clarified, errors in the scripts developed can be directly revising the code.

#### 3 Results and Discussion.

The lift coefficient curves are shown in Fig. 6 shows that the addition of the porous plate has a clear effect in the slope of the linear part of the curve experiments with a little increase, without significant changes in the angle of maximum lift coefficient CLmax. The angle of attack for zero lift is always the same, -6°. This result is important because suggests an increase of the effective aspect ratio by moving the tip vortex in the spanwise direction away from the wing tip. This vortex movement has a key effect in the noise generated by the tip vortex/wing tip interaction. Figure 5 shows the effective aspect ratio calculated from the results using the inclination of the CDxCL2 at the linear range. From these results is noted that the effective aspect ratio increase is a function of the porosity and the porosity strip size (Ps). With a large Ps there is a formation a vortex at the edge of the plate which imparts the porosity effect in changing the wing tip vortex. There is

an increase of the maximum lift coefficient CLmax with the width of the porous plate. This value is equal to 1.225 for the baseline case and 1.342 for the 70mm case that means an increment of 9.6%. The attach case also have a slight increment of the slope, but it is less than the increment that would be achieved with the same plate in the standard configuration. The effects of porosity in the drag polar can be seen in Fig. 7. There is an improvement of the drag polar with the increase of the porosity strip width mainly due to the increase in lift off the linear range. The drag coefficient is bigger for all the angles of attack, due to the increase of pressure drag as confirmed by the increase on CD for zero lift when compared with the baseline wing as shown in Fig. 7. This increase is probably due the pressure drop imposed to the flow passing through the perforated plate producing an axial force. The increment of the drag with the introducing of porous devices also was confirmed in other works [2]. The attach case does not follow this rule, the drag coefficient is almost the same that for the baseline case. The immediate conclusion is that the increment of the CD has a stronger effect than the increment of the CL. This diminution of efficiency would be very adverse for the case of a wing, but for a flap is less important as in landing or taking-off. During the landing phase, when the flap is at maximum deflection, drag increment may be beneficial to decelerate the aircraft as far as a flap side-edge noise reduction is achieved.

### 3.1 Hotwire Measurements

The anemometer of three wires allows measuring several quantities of the flow, not only the velocity. It is possible to measure the turbulence through the standard deviation of the flow, as well as moments of higher order (Reynolds stresses). Nevertheless, due to the limitations of the Matlab R code that only calculates over the average values, this information is not provided. It is possible to modify the code to calculate also the moments or higher order in future upgrades. The vorticity is calculated using a simple algorithm in Matlab. This algorithm seems to achieve logical results, but a complete validation is needed to

ensure the accuracy of the results. The subsections show figures with the magnitudes calculated, axial velocity, transversal velocity and vorticity, for all the cases. The second part realizes an analysis of the vortex, comparing the values of some important variables for each case. The measures are taken with a Reynolds of approximately  $4 \times 10^5$  and all of the magnitudes presented are non-dimensional, using U1 and c. The axial velocity is the most relevant quantity in the study of the flow field. The most immediate effect of the porous plate is to convert the "jet-like" vortex into a "wake-like" vortex, that is, from a vortex core with high velocity to a vortex core with lower velocity [1]. This effect is more pronounced with the increment of the size of the plate. It is important to taking into account some advices before the analysis of the graphics. There are two different scales, one bigger for the grids POROS, 2CHORD2 and SINGLE and one smaller for FINE (Fig. 8a) and FINE2. The color levels are also different, because it was difficult to do clear graphics with only one set of color levels. There is one for the baseline case, with a higher maximum velocity and one for all the others. The transversal velocity is represented though vectors, to give an idea about the 3D behavior of the flow field. The baseline case is the most studied, with four different experiments, two of the near field (x/c = 0.3) and two of the "far" field (x/c = 2.0). All shows the typical structure of a counter-clockwise "jetlike" vortex and a wake with lower velocity. The three cases with bigger grids have a maximum velocity around 1.3 V $\infty$ , while the case #5, with the grid FINE. has a maximum velocity of 1.418. There are two possible explanations: the improvement of the grid allows capturing a point with more elevated velocity or this fact is due to the error in the results. The maps shows a estrange diminution in the axial velocity in the right side of the vortex. Maybe it is a spurious result due to the problems with the calibration. The plate of 10mm convert the vortex in a "wake-like" vortex, with lower velocity in the center (Fig. 8 (b)). The minimum non-dimensional velocity in the vortex core is 0.654. There is a not clear structure, as was seen in the baseline case. This can be due to the presence of various vortices

that still not merge in a single coherent structure [1]. The region of lower velocity in the right side remains for this case. For this size of the plate, also a single-wire measurement was performed, at x/c = 2.0. There are two regions of bigger velocity in two opposite sides of the vortex. The most reasonable explanation to this fact is that the anemometer is capturing the velocity in another axis. The case #6, with a plate of 20mm, is shown in Fig. 9(a). The vortex is weakened, with a minimum velocity of 0.473. The structure is more conventional and the region of lower velocity was not disappeared. Fig. 9(b) shows the case #4, with a plate of 30mm and a larger grid. The vortex begins to

30mm and a larger grid. The vortex begins to merge with the wake. The minimum velocity is 0.307 and the region of lower velocity is not exactly coincident with the center of rotation of the flow. The case #3, d=50mm begins to show a new behavior (Fig. 10(a)). The wake is completely merged with the vortex and the flow seems to have two different vortex structures. Nevertheless, the region of minimum velocity (0.353) remains in the place of the vortex of the previous cases.

It is not known if the mentioned structure in the near field would be benefit for noise reduction. The case #2, d=70mm, shows a reinforcement of the structure mentioned above, but the region of lower velocity is shifted to the left side (see Fig. 10(b)). This is the minimum nondimensional velocity measured in all of the experiments, 0.235. The study of the energy exchange between the wake and the vortex can be topic of study in future works. Figure 11(b) shows the attach case, that, one more time, has a completely different aspect. The vortex seems to be weakened, but the center has a bigger velocity that the flow around. The transversal velocity is also higher than for configurations with similar size of the plate. The comparison between the attach and the standard configuration suggests that the effect over the vortex is completely different.

The vortex is composed for the spinning motion of the transversal velocity, so these components are important to understand it. Ideally, the graphics would show a negative and a positive region separated for a perpendicular line at one of the axis. However, the separating line

between positive and negative regions is inclined in some cases. A roll angle of 30° was already applied to the results, but it have to be considered future improvements of this value, as well as different values for each case. All of the figures have the same color levels, and then the graphics with less variations of the flux have a very similar color. It was preferred to have this disadvantage to have problems of interpretation due to different legends. All of the cases have a very similar behavior, with little variations respect to the "ideal" case. The general tendency is a decrease of both components with the increase of the porous plate. The only strange detail is an asymmetry on the V - values. The results show systematically a higher value in the upper part than in the lower. No explanations were found for this fact. Figure 12(a) shows the profiles of W velocity for the z coordinate that passes in the vortex core. The results are divided into two graphics to improve the visualization of the results. The two measurements done for the baseline shows a good agreement. The shape of the curves is the expected, although there is some asymmetry. This is partially due to the accuracy of the grid and partially to the errors in the results. The maximum values are almost the same for the negative and the positive side. However, the curve is not symmetric. It shows a slower decrease in the right side corresponds to the area of lower axial velocity already mentioned. Figure 12(b) shows the profiles of V velocity for the y coordinate that passes in the vortex core. The non-symmetric aspect of the curves is due to the dimensions of the grids, with more space below the vortex than Nevertheless. above. there is another asymmetry, already mentioned in this subsection. The velocity V reaches a higher absolute value in the upper part than in the lower. This is probably due to an interaction with the wake.

## 3.2 Vorticity

The vorticity is the rotational of the flux and gives a measurement about how quickly the fluid is rotating. Therefore, it is the perfect variable to evaluate the vortex, leaving aside the velocity. The mathematical expression is:

$$\vec{\Omega} = \nabla \times \vec{V} = rot \vec{V} \tag{2}$$

Where  $\bar{\Omega}$  is the vorticity, V the velocity of the flow  $\nabla$  and *rot* are the vectorial operator and rotational. The hotwire probe only give results in a y - z plane, then only it is possible to calculate the vorticity normal to this plane, that is, the vorticity in the x-axis:

$$\omega_{x} = \frac{\partial W}{\partial Y} - \frac{\partial V}{\partial Z} \tag{3}$$

The graphics shows the non-dimensional vorticity, using c/U1 as the characteristic time. This value represents the time for an undisturbed particle to go across the wing and the parameters for the calculations are presented in Table 2. There is a big discrepancy between the values that led to use two set of colors levels, as it was done with the U component of the velocity. Figure 13 contains the five cases with more elevated velocity, with a scale of color levels until 80. There is several interesting information in this graphics. The maximum vorticity of the baseline case is around 47 for the two larger grids (POROS and 2CHORD2), while for the FINE grid increases until 80. It is have to be determined if this result is spurious or if it is an improvement due to the better grid. The attach case have the same maximum level than the baseline. This reaffirms the theory of that this configuration does not weak the vortex as the others. The case #7, with d=10mm shows an important decrease until 37. Figure 14 shows the vorticity for the rest of the cases, with color levels until 20. The plate of 20mm presented a maximum of 18.8 and the other three cases similar values around 9. This fact suggests that the weakening of the vortex is approaching an asymptotical value. The graphic of the case #2 (70mm) shows an interesting result. The area of maximum vorticity is roughly in the same place, while in the Fig. 10 it can be seen that the minimum velocity was shifted to the left side. This suggests that this area of minimum velocity is still a wake that has been reinforced with the interaction with the vortex.

#### **5 Conclusions**

The work present presents several discovering about the wing tip flow field with a porous plate. The porous plate produces an increment in the lift, higher when wider is the plate. This increment is countered with an increase of the drag that finally results in a diminution of the efficiency L/D. The attach case have a different behavior, as in another aspects of the results. The addition of the porous plate provokes immediately the change from a structure "jet-like" (higher velocity in the core) to a "wake-like" structure (lower velocity in the core). The vortex is weakened in all of the parameters taken to its study: maximum axial velocity, maximum transversal velocity and maximum vorticity. From d=30mm, it seems that the diminution approaches to an asymptotic value. The attach case does not modify the vortex in the same way. It seems that the structure also changes to "wake-like", but this is not completely confirmed. The vorticity does not have significant changes that suggest the diminution in the axial velocity is only a pressure drop due to the extra drag of the plate. The wake and the vortex seems to merge for d=50mm and d=70mm. This physical process and its consequences for the noise should be investigated in future works.

#### 6 References

- 1 Anderson, D. E. A. and Wright, C. T. (2000). Experimental study of the structure of a wingtip vortex.
- 2 Angland, D. (2008). Aerodynamics and Aeroacoustics of Flap Side-Edges. PhD thesis, University of Southampton, Faculty of Engineering, Scienceand Mathematics, School of Engineering Sciences.
- 3 Brooks, T. F. and Humphreys, W. M. (2003). Flap edge aeroacoustic measurements and predictions. Journal of Sound and Vibration, 261:31–74.
- 4 Catalano, F. (2004). The new closed circuit wind tunnel of the aircraft laboratory of university of São Paulo. In 24th ICAS 2004 Congress.
- 5 Catalano, F. M., Vanucci, P., and Correa, L. G. N. (2012). Wind tunnel testing of porous devices for the reduction of flap side-edge noise. In 28th ICAS 2012 Congress.
- 6 Choudhari, M. M. and Khorrami, M. R. (2003). Computational study of porous treatment for

- altering flap side-edge flowfield. AIAA-2003-3113.
- 7 Dobrzynski, W. (2010). Almost 40 years of airframe noise research: What did we achieve? Journal of Aircraft, 47(2):353–367.
- 8 Gerz, T., Holzäpfel, F., and Darracq, D. (2002). Commercial aircraft wake vortices. PERGAMON Progress in Aerospace Sciences, 38:181–208.
- 9 Hong joon Park, M. (2006). Three component velocity measurements in the tip vortex of a micro-air-vehicle. Master's thesis, Air Force Institute of Technology.
- 10 Khorrami, M. R. and Choudhari, M. M. (2003). Application of passive porous treatment to slat trailing edge noise. Technical report, NASA Langley Research Center.
- 11 Strett, C. L. (1998). Numerical simulation of a flap-edge flowfield. AIAA-98-2226.
- 12 Catalano, F.M. & Carmo, M: The Scientific and Technological Projects Developed Between University of Sao Paulo and Embraer and its Impact on Engineering Education, *International Journal of Engineering Education* Vol. 29, No. 6, pp. 1–9, 2013 0949-149X/91 \$3.00+0.00

## **Copyright Statement**

The authors confirm that they, and/or their company or organization, hold copyright on all of the original material included in this paper. The authors also confirm that they have obtained permission, from the copyright holder of any third party material included in this paper, to publish it as part of their paper. The authors confirm that they give permission, or have obtained permission from the copyright holder of this paper, for the publication and distribution of this paper as part of the ICAS 2014 proceedings or as individual off-prints from the proceedings.

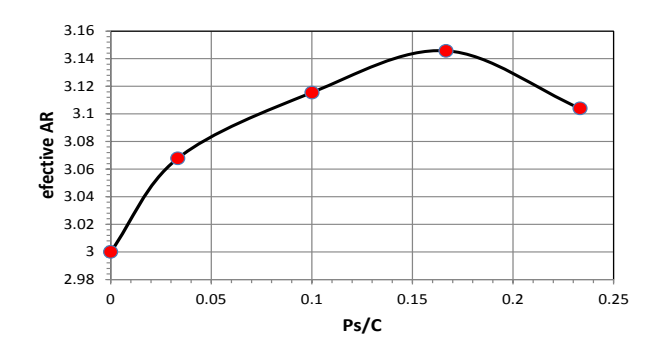


Fig. 5 Effective aspect ratio.

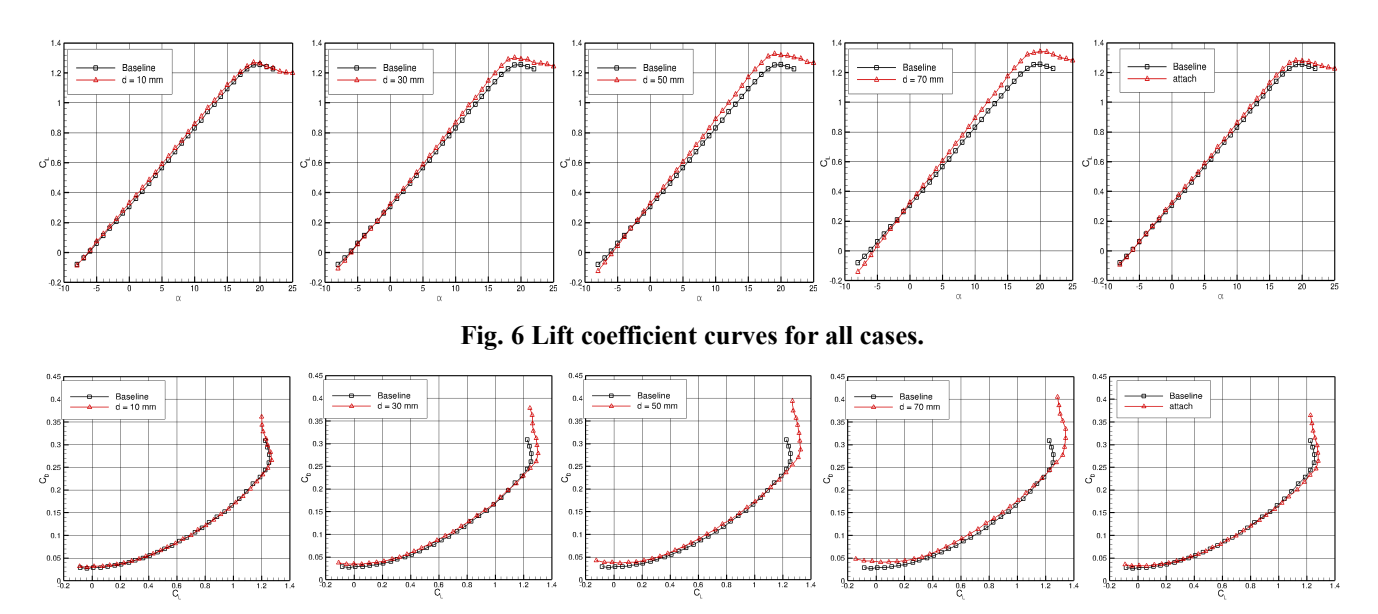


Fig. 7 Drag polar for all cases.

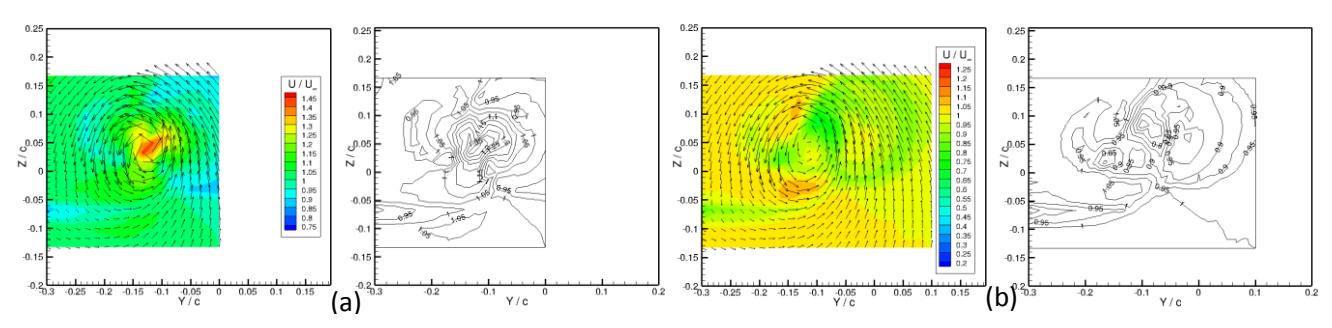


Fig. 8 (a) Case #5, baseline, grid FINE d=0mm, x/c=2.0; (b) Case #7 grid FINE2 d=10mm, x/c=0.3.

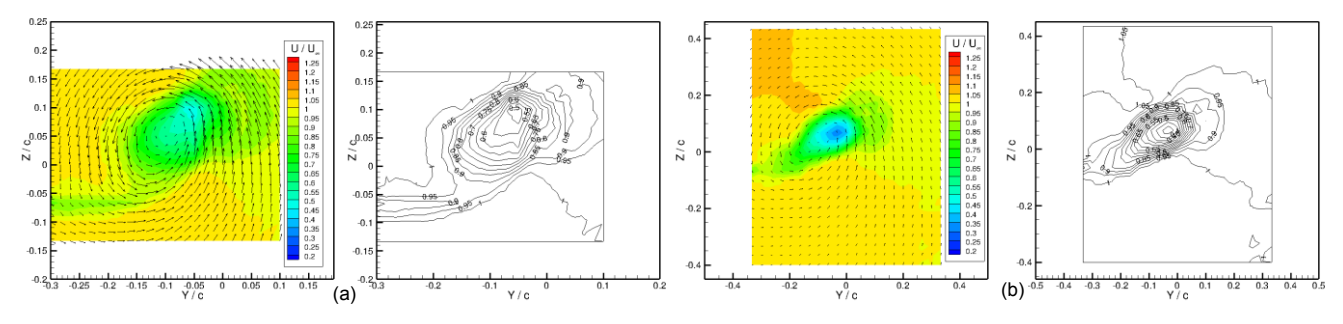


Fig. 9 (a) Case #6, grid FINE2 d=20mm, x/c = 0.3; and (b) Case #4, grid POROS. d=30mm x/c = 0.3.

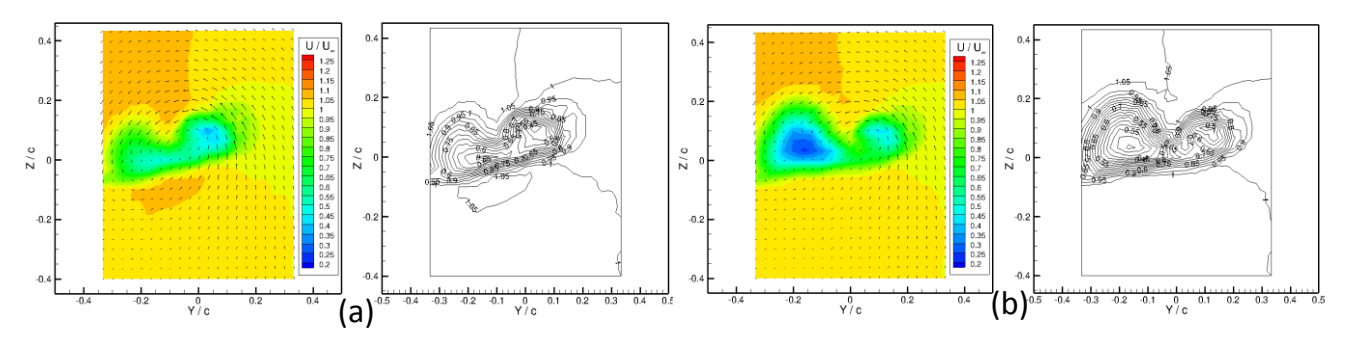


Fig. 10 Case #3, d=50mm, x/c=0.3, grid POROS. U velocity. Case #2, d=70mm, x/c=0.3, grid POROS.

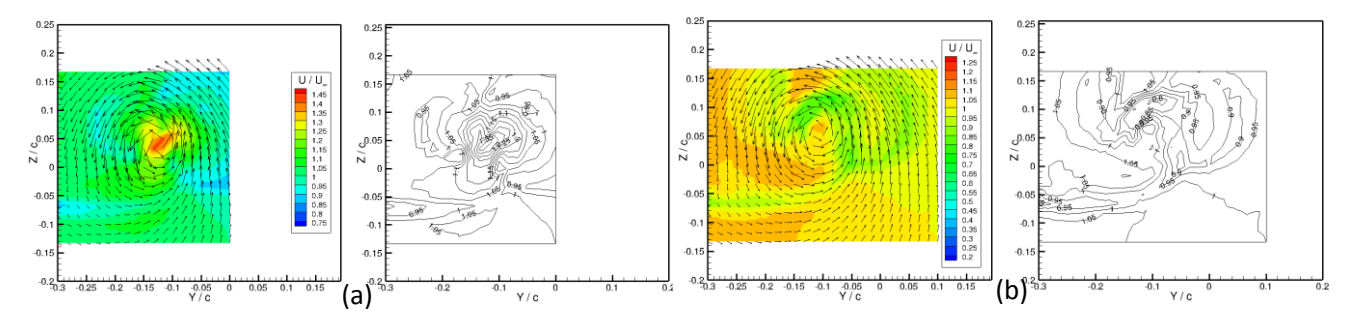


Fig. 11 (a) Case #5, baseline, grid FINE d=0mm, x/c = 2.0, Case #8, attach, d=25mm, x/c = 0.3, grid FINE2.

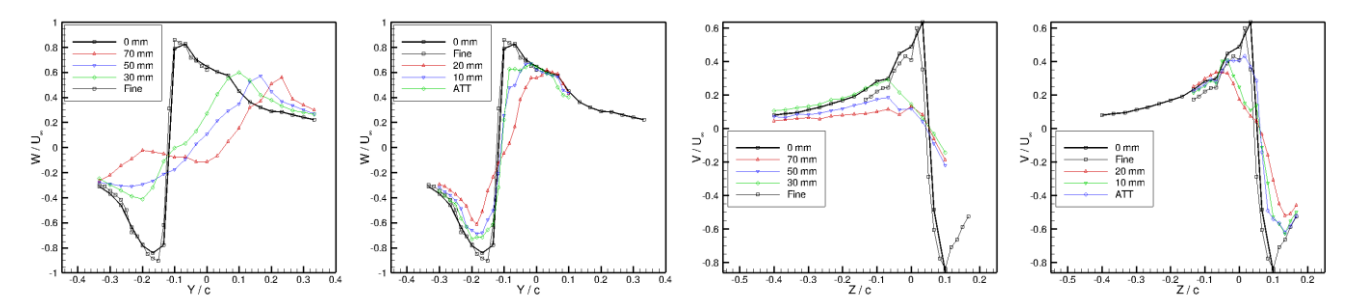


Fig. 12 Profiles of W velocity and V velocity.

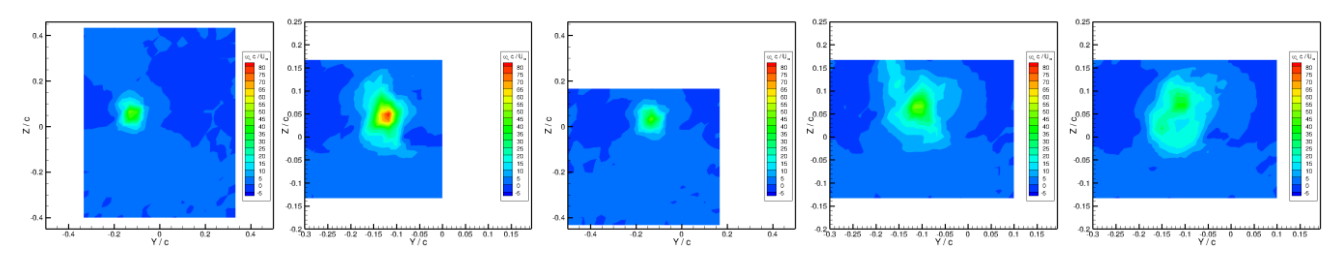


Fig. 13 Vorticity in the x-axis x for cases #1, #5, #9, #8, #7.

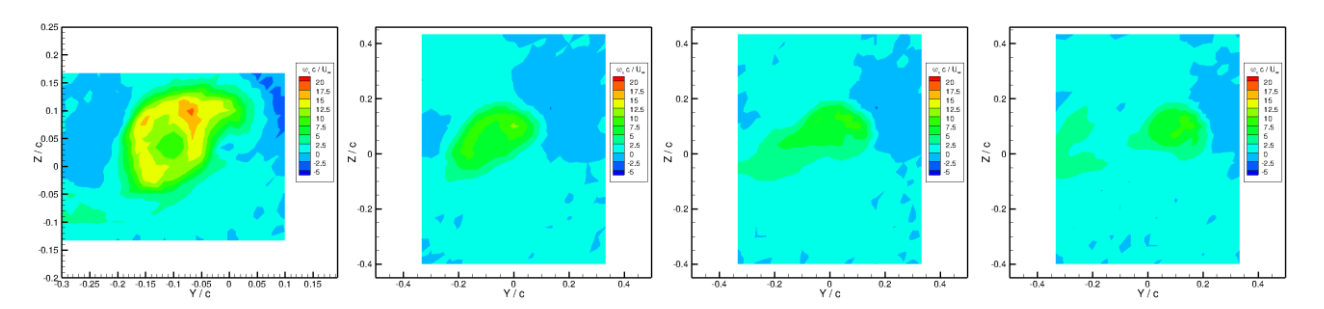


Fig. 14 Vorticity in the x-axis x for the cases, #6, #4, #3, #2.

Table 2 Vortex parameters for the 12 cases studied

d	#	$U_{\infty}$	$\frac{U_{max}}{U_{\infty}}$	$\frac{U_{min}}{U_{\infty}}$	$\frac{\sqrt{(V^2+W^2)_{max}}}{U_{\infty}}$	$(\omega_x)_{max}$	$\frac{(\omega_x)_{max}c}{U_{\infty}}$
0	1	18.716	1.321	0.802	0.985	2917.826	46.769
0	5	21.667	1.418	0.829	1.038	5774.730	79.956
0	9	22.055	1.308	0.858	0.924	3466.911	47.159
0	10	23.568	1.363	0.874	-	-	-
10	7	22.364	1.078	0.654	0.804	2758.525	37.005
10	12	23.164	1.099	0.874	-	-	-
20	6	22.414	1.049	0.473	0.715	1395.580	18.679
30	4	18.994	1.064	0.307	0.684	670.060	10.583
50	3	17.899	1.096	0.353	0.664	556.024	9.319
50	11	23.433	1.032	0.689	-	-	-
70	2	18.289	1.073	0.235	0.626	525.228	8.615
25	8	20.405	1.104	0.776	0.803	3288.864	48.355